Earth and Planetary Science Letters 578 (2022) 117306

Contents lists available at ScienceDirect

Earth and Planetary Science Letters

www.elsevier.com/locate/epsl

Prevalence of updip rupture propagation in interplate earthquakes along the Japan trench

Keisuke Yoshida [a,*], Naoki Uchida [a], Hisahiko Kubo [b], Ryota Takagi [a], Shiqing Xu [c]

[a] Research Center for Prediction of Earthquakes and Volcanic Eruptions, Graduate School of Science, Tohoku University, Sendai, Japan
[b] National Research Institute for Earth Science and Disaster Resilience, Tsukuba, Japan
[c] Department of Earth and Space Sciences, Southern University of Science and Technology, Shenzhen, China

ARTICLE INFO

Article history:
Received 11 February 2021
Received in revised form 10 November 2021
Accepted 16 November 2021
Available online 25 November 2021
Editor: R. Bendick

Keywords:
rupture directivity
interplate earthquake
Japan trench
deep creep
fluid migration
subduction zone

ABSTRACT

The development of seafloor seismic observations facilitates the reliable estimation of rupture directivities from offshore earthquakes. We used seismic waveforms obtained by a new seafloor seismic network (S-net) and stations on land to systematically examine the rupture directivities of interplate earthquakes along the Japan trench. We estimated the rupture directions of 206 M_w 3.5–5 events, most of which occurred near the base of the seismogenic zone. We found that most earthquake ruptures (>80%) were directional, primarily propagating in the updip direction. This tendency favoring updip rupture cannot be explained by the effect of the bimaterial interface. The prevalence of updip rupture in the data suggests that deep aseismic slip and upward fluid migration along the plate interface affected earthquake ruptures in the subduction zone. The updip ruptures redistributed the accumulated shear stress from the base of the seismogenic zone to shallow large seismic patches. Furthermore, the updip ruptures may open paths for deeper fluids to migrate further upward along the plate interface. Both the stress redistribution and upward fluid migration may facilitate the occurrence of shallow megathrust earthquakes.

1. Introduction

A physical understanding of earthquakes involves not only the static characteristics of the rupture but also the dynamics. Ruptures of small earthquakes (M<5) are often approximated by symmetrical expansions of circular fault patches (e.g., Sato and Hirasawa, 1973). However, according to systematic investigations, many earthquake ruptures propagate asymmetrically (McGuire et al., 2002; Chounet et al., 2018; Yoshida, 2019). Rupture directivity is a fundamental characteristic of earthquake growth and is essential for improving our current physical understanding of earthquakes. Furthermore, rupture directivity provides information regarding the stress redistribution process that occurs along the fault.

The effect of material contrast across a fault interface (bimaterial effect) has received attention for its role in understanding earthquake rupture direction (Weertman, 1980; Shi and Ben-Zion, 2006). When an in-plane subshear rupture propagates in the slip direction of the compliant material side, a dynamic reduction in normal stress occurs, leading to lower frictional resistance and a higher rupture speed in this direction. The bimaterial effect leads to a hypothesis that a preferable rupture direction may exist, controlled by the elastic contrast, which is independent of the earthquake size. Several reports have concluded that the observed dominant rupture direction of small earthquakes on the San Andreas fault is consistent with the prediction from the bimaterial effect (e.g., Lengliné and Got, 2011; Kane et al., 2013). However, others argue that effects other than the bimaterial effect, such as spatial variations in background stress, play more crucial roles in earthquake rupture directivity (Harris and Day, 2005; Kane et al., 2013). It is important to assess the above hypothesis by incorporating reliable data from different tectonic settings as this hypothesis is involved in predicting the rupture directions of future earthquakes.

Currently, the rupture characteristics of interplate earthquakes have been examined in detail, mostly for a small number of large earthquakes in subduction zones (Yamanaka and Kikuchi, 2004; Ye et al., 2016). However, the rupture characteristics of a large amount of small- to moderate-sized earthquakes have not been thoroughly studied, despite their potential to improve the significance level of the direction estimates by increasing the sample size. The reliability of the rupture-direction measurement of small earthquakes, however, highly depends on the azimuthal coverage of observations. Poor azimuthal coverage makes reliable estimation difficult. Interplate earthquakes in subduction zones mostly occur beneath

* Corresponding author.
E-mail address: keisuke.yoshida.d7@tohoku.ac.jp (K. Yoshida).

https://doi.org/10.1016/j.epsl.2021.117306

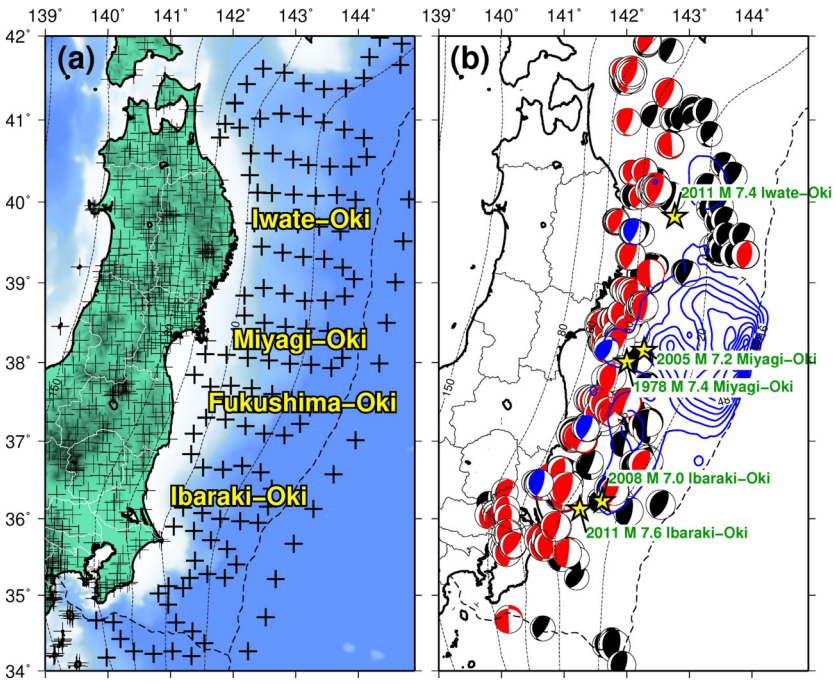

Fig. 1. The distribution of earthquakes and seismic stations in the study area. (a) Distribution of on-land and S-net seismic stations. The thick and thin crosses indicate S-net stations and those on land, respectively. (b) The distribution of target interplate earthquakes with their focal mechanisms indicated by beach balls. Red beach balls indicate earthquakes for which rupture parameters were estimated, while black beach balls indicate earthquakes for which rupture parameters were not estimated. Blue beach balls indicate earthquakes for which the results are shown in Fig. 2. The contour lines in blue denote the coseismic slip distribution of the 2011 Tohoku-Oki earthquake determined by Iinuma et al. (2012). Yellow stars represent the five $M > 7$ interplate earthquakes (1978 M 7.4 Miyagi-Oki, 2005 M 7.2 Miyagi-Oki, 2008 M 7.0 Ibaraki-Oki, 2011 M 7.4 Iwate-Oki, and 2011 M 7.6 Ibaraki-Oki earthquakes) that occurred near the earthquakes analyzed in this study. Dotted contours indicate the depth to the upper plate interface of the subducting Pacific plate, from Nakajima et al. (2009) and Kita et al. (2010). (For interpretation of the colors in the figure(s), the reader is referred to the web version of this article.)

the ocean, where seismic stations are usually scarce, causing a paucity of data.

The present study systematically estimates the rupture directivity of interplate earthquakes (*Mw* 3.5–5) along the Japan trench to investigate earthquake rupture dynamics. Many large earthquakes have occurred in the offshore area along the Japan trench and caused disasters in Japan, including the 2011 M 9 Tohoku-Oki earthquake. Recently, the Seafloor observation network for earthquakes and tsunamis along the Japan Trench (S-net), was installed along the Japan trench by the National Research Institute for Earth Science and Disaster Resilience (NIED) (Fig. 1a; Aoi et al., 2020). Seismic waveform data from September 2016 onwards are available online (https://www.seafloor.bosai.go.jp/). Fig. 1(a) shows the distribution of S-net stations, surrounding the epicenters of the recent interplate earthquakes. Waveform records from the S-net and stations on land provide unique observations with good azimuthal coverage for interplate earthquakes occurring beneath the ocean. It is thereby possible to systematically examine the rupture directivity of small interplate earthquakes along the Japan trench.

2. Data and methods

This study uses waveforms obtained from the seismic network composed of stations from the Japan Meteorological Agency (JMA), national universities, Hi-net (NIED, 2019a), F-net (NIED, 2019b), V-net (NIED, 2019c), and S-net (NIED, 2019d), as shown in Fig. 1(a), after removing their instrument responses. Initially, interplate earthquakes were selected (section 2.1), and the apparent moment rate functions (AMRFs) were estimated based on the empirical Green's function (EGF) (section 2.2). Next, the rupture direction was estimated by fitting the simple rupture model described by Haskell (1964) to the apparent rupture durations obtained from the AMRFs (section 2.3).

2.1. Selection of interplate earthquakes

The F-net moment tensor catalog (https://www.fnet.bosai.go.jp/event/dreger.php?LANG=en) and JMA unified earthquake catalog (https://www.data.jma.go.jp/svd/eqev/data/bulletin/hypo_e.html) were used to select the interplate earthquakes. The F-net moment tensor catalog lists the moment tensors of earthquakes with M_w greater than about 3.5 in and around Japan, while the JMA unified catalog includes location data for earthquakes with smaller magnitudes. The data period extended from August 2016 to December 2019, for which the S-net station seismograms were also available.

In total, 420 interplate events (target events) were selected using the F-net moment tensors based on the criteria used by Asano et al. (2011) and Hasegawa et al. (2012) (Fig. 1b). The requirements were as follows: a rake angle of $> 0°$, a focal mechanism three-dimensional rotation angle relative to a reference interplate earthquake (strike: 195°, dip: 15°, rake: 90°) of $< 35°$, and a depth separation of < 20 km between the centroid and the plate interface (Nakajima et al., 2009). To estimate the directivity of the target events, we selected 660 smaller nearby earthquakes (EGF events) and used their waveform data for waveform deconvolution. These EGF events satisfied the following two criteria: (1) the hypocentral distance from the target event was < 3.0 km according to the JMA unified catalog, and (2) the magnitude was 1–2 magnitudes smaller than the target earthquake. Each target earthquake may have multiple EGF events. Note that the hypocenter locations of the offshore earthquakes had relatively large estimation errors, and thus, earthquakes located far from the target earthquake may be selected as EGF events on occasion. However, these were removed during the waveform deconvolution procedure, as described in section 2.2.

2.2. Determination of the apparent moment rate function and source duration

For waveform deconvolution, we followed the procedure of Yoshida (2019), which adopted the iterative time-domain method of Ligorría and Ammon (1999). The transverse components of direct S-waves were used. For the S-net seismometers, the orientations determined by Takagi et al. (2019) were used. We first applied a low pass filter to the waveforms of the target and the EGF events. The cut-off frequency (f_l) should be higher than the source corner frequency of the target earthquake (f_{cS}). Based on the source model of Sato and Hirasawa (1973), the S-wave source corner frequency is related to the stress drop $\Delta\sigma$ as follows:

$$f_{cS}(\Delta\sigma) = kV_s\left(\frac{16}{7}\frac{\Delta\sigma}{M_0}\right)^{\frac{1}{3}}, \quad (1)$$

where V_s is the S-wave velocity, and M_0 is the seismic moment. We assumed $k = 1.9$ corresponding to the situation where the rupture speed is 0.8 times V_s. The typical value of $\Delta\sigma$ for interplate earthquakes is 3 MPa (Kanamori and Anderson, 1975). We used $f_l = f_{cS}(\Delta\sigma = 100$ MPa). Thus, f_l is sufficiently higher than the typical source corner frequency of interplate earthquakes, $f_{cS}(\Delta\sigma = 3$ MPa).

The AMRFs were then derived by deconvolving the waveforms of the target events using the EGFs with a positive value constraint. Synthetic waveforms for the target events can be obtained by convolving the derived AMRFs with the EGFs. When a synthetic waveform does not reproduce the observed waveform adequately, it implies that the EGF was inappropriate for the observed waveform. Waveform deconvolution thereby naturally removes such inappropriate EGFs (Abercrombie, 2015). We discarded the AMRF if the synthetic waveform reproduced less than 80% of the observed waveform measured in the variance reduction. If the number of stations with AMRFs from a single EGF event was less than eight, we discarded the AMRFs from that EGF event. The corner frequency (Andrews, 2013) f_c for each AMRF was computed in the time domain as $f_c = \frac{1}{2\pi}\sqrt{\frac{\int \dot{A}^2(t)dt}{\int A^2(t)dt}}$, where $A(t)$ is the time series of the AMRF amplitude. The apparent source durations were obtained as $T_d = \frac{1}{2f_c}$. Note that the simple inverse relationship between f_c and T_d does not hold for complex AMRFs with multiple pulses. However, our manual inspection confirms that the effects of source complexity are only minor because of the relatively low-frequency band used here. Figs. 2 and 3 show examples of the azimuthal distributions of the AMRFs and the source durations.

AMRFs were obtained from more than 15 different stations for 206 of the initial 420 target earthquakes (Fig. S1), and their rupture directivities were examined in detail. The rupture directions of the remaining 214 earthquakes could not be estimated owing to an insufficient number of stations with available AMRFs. For the 214 events, the minimum distances of the EGF events tended to be larger (>1.5 km) than those of the other 206 events (0–1.5 km) (Fig. S1). This tendency implies that the scarcity of AMRFs for the 214 events was caused by the absence of an appropriate EGF event, probably because the candidate EGF events were too far to assume the same path effect. This natural selection of analyzed events does not bias the statistical tendency of the rupture directions because the presence or absence of nearby (<1.5 km) small events is not related to the rupture direction.

2.3. Determination of rupture directivity

To estimate the rupture directivity, we followed the procedure described by Yoshida et al. (2019), which uses the one-dimensional unilateral rupture model (Haskell, 1964) to compute the apparent rupture duration:

$$T_{d0}^{model} = T_0\left(1 - \eta\,\vec{R}\cdot\vec{U}\right). \quad (2)$$

Here, T_0 is the actual rupture duration, η is the speed of the unilateral rupture divided by V_S, and $\vec{R}$ and $\vec{U}$ represent the unit vectors of the rupture propagation and the ray direction at the source, respectively. For simplicity, the shape of a theoretical AMRF is assumed to be a symmetrical triangle with a base of T_{d0}^{model}. We applied the same low pass filter to the synthetic triangle and obtained the duration T_d^{model} as the same way used for observed AMRFs.

We grid-searched for the combination of $\vec{R}$, T_0, and η that best explained the obtained apparent source durations. $\vec{R}$ was located on the west-dipping nodal planes of focal mechanisms that corresponded to the plate boundary. The evaluation function is as follows:

$$Var_{uni} = \frac{\sum_{i=1}^{n}\left(T_d^{model}\left(T_0, \eta, \vec{R}, \vec{U_i}\right) - T_{di}\right)^2}{n}, \quad (3)$$

where T_{di} and $\vec{U_i}$ are T_d and $\vec{U}$, respectively, of the i-th AMRFs, and n is the number of the AMRFs. $\vec{U_i}$ was computed based on the one-dimensional velocity model of Ueno et al. (2002). We changed the apparent speed ratio η (0–1.0) by dividing the interval by 0.05 and the rupture propagation direction (10–360°) that determined $\vec{R}$ by dividing the interval by 10°. The rupture duration T_0 was searched from 100 points, evenly dividing the interval on a logarithmic scale between 0.1 and ten times the mean value of T_{d_i}. Ruptures may propagate faster than the S-wave velocity in the Mode II direction (Andrews, 1976). However, we considered the likelihood of $\eta > 1$ to be low because Var_{uni} increased beyond $\eta = 1$ for almost all cases in the dataset used in this study.

The residual of Eq. (3) was compared with that of the constant source duration $\overline{T_d}$ case (we referred to the model as the "non-directional model").

$$Var_{mean} = \frac{\sum_{i=1}^{n}\left(\overline{T_d} - T_{di}\right)^2}{n} \quad (4)$$

$$VR = 100\% \times \left(1 - \frac{Var_{uni}}{Var_{mean}}\right) \quad (5)$$

If a unilateral rupture more suitably models the duration data, VR will approach 100%. $\overline{T_d}$ was determined during the above grid-search procedure (best-fit value when $\eta = 0$).

We computed the Akaike Information Criterion (AIC) (Akaike, 1974) by assuming that measurement errors in the apparent duration followed a Gaussian distribution, as $AIC = n\ln 2\pi + n\ln Var + 2(m+1)$. Var and m are the mean squared residual and the number of model parameters, respectively. $m = 1$ and $m = 3$ were used for the non-directional model and the unilateral rupture model, respectively. We computed the difference $\Delta AIC = AIC_{mean} - AIC_{uni}$, where AIC_{mean} and AIC_{uni} are the AICs of the non-directional model and the unilateral rupture model, respectively.

We estimated the uncertainty range of the directivity parameters for each earthquake by conducting the above procedure on 1,000 simulated datasets based on bootstrap re-sampling of the duration data. We determined the 95% confidence intervals of $\vec{R}$, T_0, and η. Figs. 2(c) and 3 include examples of the best-fit values and 95% confidence intervals of the rupture azimuths determined using this method.

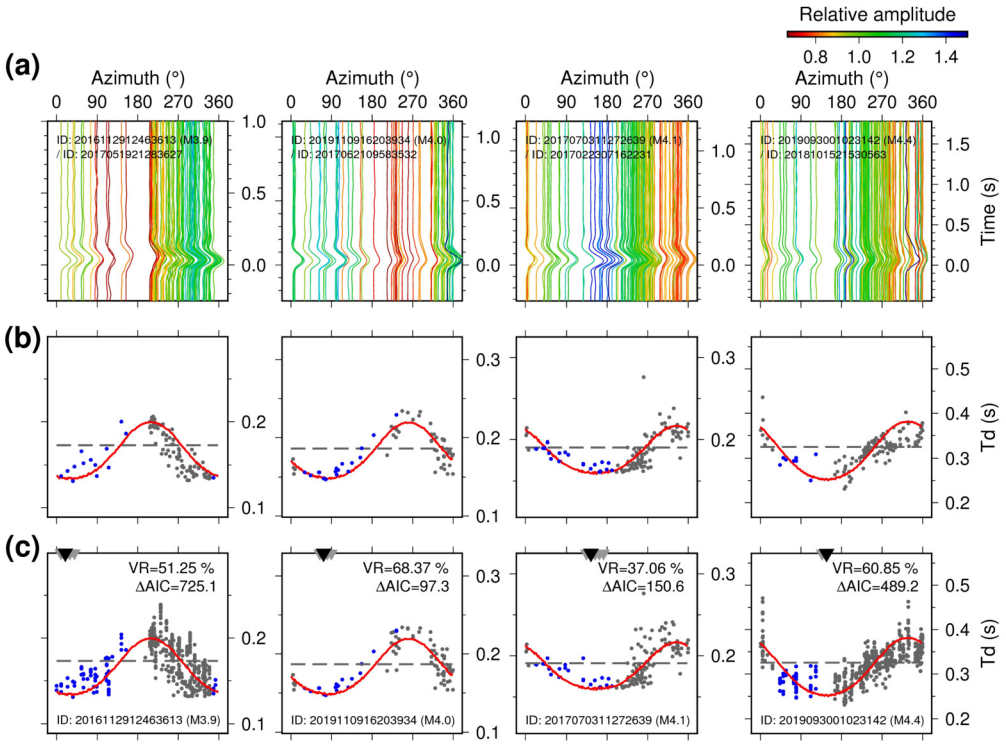

Fig. 2. (a) Examples of the AMRF azimuthal distributions for events shown in Fig. 1(b) from north to south. The different colors indicate the relative maximum amplitude as per the scale provided on the top. (b), (c) Examples of AMRF corner frequencies from a single EGF event and those compiled from multiple EGF events, respectively. Azimuth is measured in degrees, clockwise from the north. Blue dots indicate the results from S-net stations, and gray dots indicate those from stations on land. Black triangles indicate the best-fit azimuth of rupture propagation based on the unilateral rupture model. Gray triangles indicate the results from bootstrap re-sampling. The red curve and the dashed gray line indicate the computed azimuthal dependences of the apparent source duration from the best-fit unilateral model and the non-directional model, respectively. Event IDs (from the JMA catalog) are shown in the lower-left corner of each frame with the moment magnitude (from the F-net catalog).

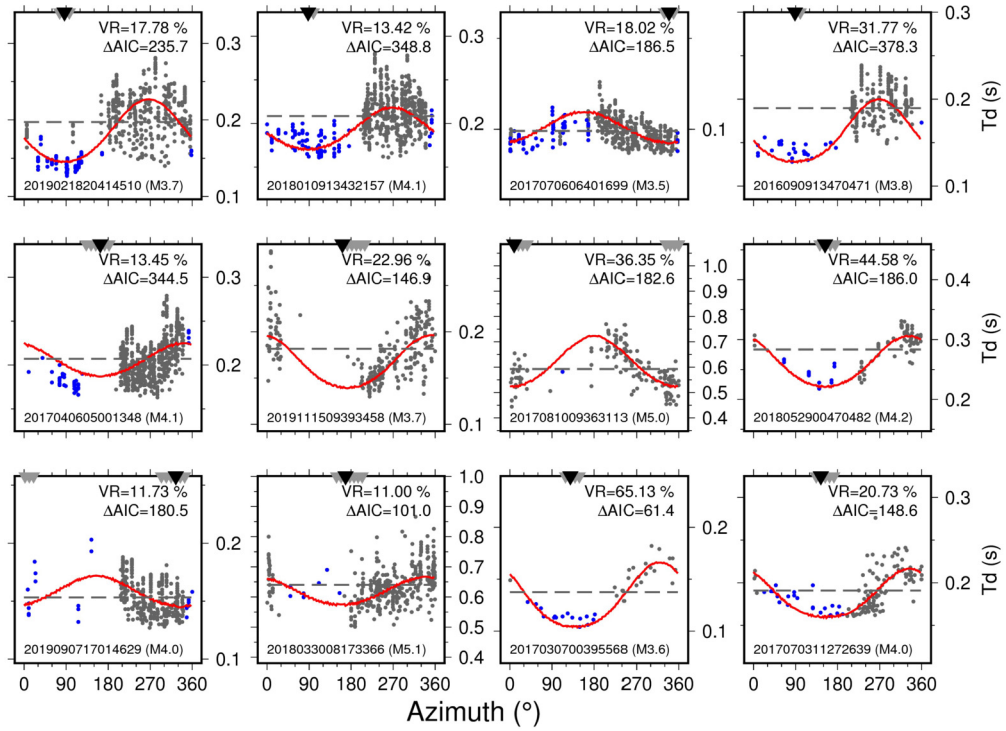

Fig. 3. Other examples of AMRF durations. Blue and gray dots indicate results from S-net stations and those from stations on land, respectively. Black triangles indicate the best-fit rupture propagation azimuth, and gray triangles show the results of the bootstrap re-sampling. The red curve and dashed gray line indicate the computed azimuthal dependence of the apparent source duration from the best-fit unilateral and non-directional models. Event IDs (from the JMA catalog) are shown in the lower-left corners with the moment magnitude (from the F-net catalog).

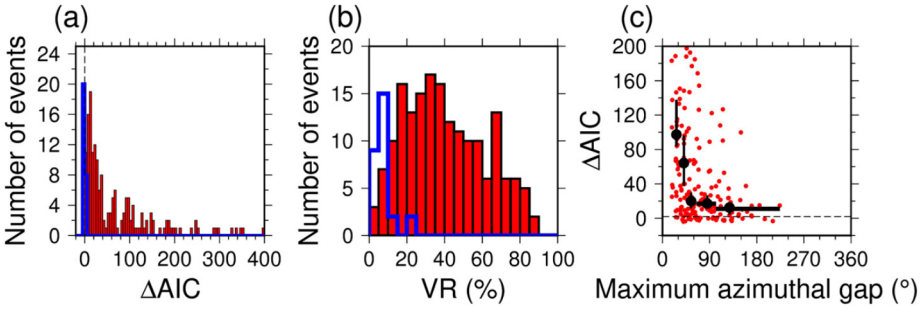

Fig. 4. Results of applying the unilateral rupture model to the dataset used in this study. (a) and (b): Frequency distributions of ΔAIC and VR, respectively. The red bars denote the results with $\Delta AIC \geq 2$ and blue bars denote those with $\Delta AIC < 2$ (including negative values). (c): Relationship between ΔAIC and the maximum azimuthal gap of the corner frequency data used to estimate the rupture parameters. Vertical lines indicate 95% confidence intervals of the median value based on bootstrap re-sampling in each bin with the same number of events (n=41). Horizontal lines indicate the ranges of the maximum azimuthal gap in each bin.

3. Results

We obtained the rupture parameters for 206 earthquakes (*Mw* 3.5–5), for which the $\Delta AICs$ are shown in Fig. 4(a) by their frequency distribution. ΔAIC was positive in 186 out of the 206 earthquakes, indicating that 186 earthquakes were better modeled by the unilateral rupture model than by the non-directional model. $\Delta AIC > 2$ in 178 earthquakes; that is, the unilateral rupture model was a better model for these earthquakes based on the 95% confidence interval. For the 178 events with $\Delta AIC > 2$, VR was larger than 25% for ∼75% of the events, and VR was larger than 40% for ∼40% of the events (Fig. 4b). The mean ΔAIC decreased with an increasing maximum azimuthal gap of the duration data (Fig. 4c), implying that $\Delta AIC < 0$ does not necessarily reflect a non-directional event but is due to limited data available for resolving the directivity effect.

Fig. 5 shows the obtained rupture parameters for events with $\Delta AIC > 2$. The estimated value of η is shown in Figs. 5(a) and (b) when the 95% confidence interval was less than 0.2. η mostly ranged from 0.1 to 0.6 (Fig. 5a). η was variable, and the number of samples for the larger earthquakes was smaller than others but may decrease with the moment magnitude (Fig. 5b). Source duration T_0 mostly ranged from 0.1 to 1 s and increased by the power of 1/3 of the seismic moment (Fig. 5c). This relationship is consistent with the self-similarity of earthquakes (Kanamori and Anderson, 1975). No clear dependence of the characteristic source duration $T_0/M_0^{\frac{1}{3}}$ on the centroid depth was obtained (Fig. 5d).

A clear trend for the rupture propagation direction was observed. Fig. 6 shows the rupture propagation directions of the 148 earthquakes that satisfied the following two conditions: the 95% confidence interval of the rupture propagation direction was less than 45° and $\Delta AIC > 2$. The frequency distribution (Fig. 6a) indicates that ruptures of most of the earthquakes (∼80%) were oriented eastward rather than westward. The ruptures of most of the interplate earthquakes along the Japan trench propagated in the updip direction. This trend appears to be independent of earthquake magnitude (Fig. 6b) and centroid depth (Fig. 6c), barely changing even if different criteria were adopted for the results. Fig. S2 shows 178 results with a 95% confidence interval for a rupture azimuth of less than 90° regardless of ΔAIC, and Fig. S3 shows 114 results with a 95% confidence interval for a rupture azimuth of less than 45° and $\Delta AIC > 20$.

The predominance of updip rupture was most comprehensible in the Iwate-Oki and Miyagi-Oki regions (Figs. 6f and g). The same trend was also observed in the Fukushima- and Ibaraki-Oki regions (Fig. 6h), which are located to the north of the northeastern limit of the Philippine Sea plate (broken curve in Fig. 6d). In the northernmost region and southernmost region (south of the northeastern limit of the Philippine Sea plate), the dominant rupture directions are south-by-southeast (SSE) (Figs. 6e and i). Although this SSE direction is roughly consistent with the predominance of updip rupture, the fault-strike component is large.

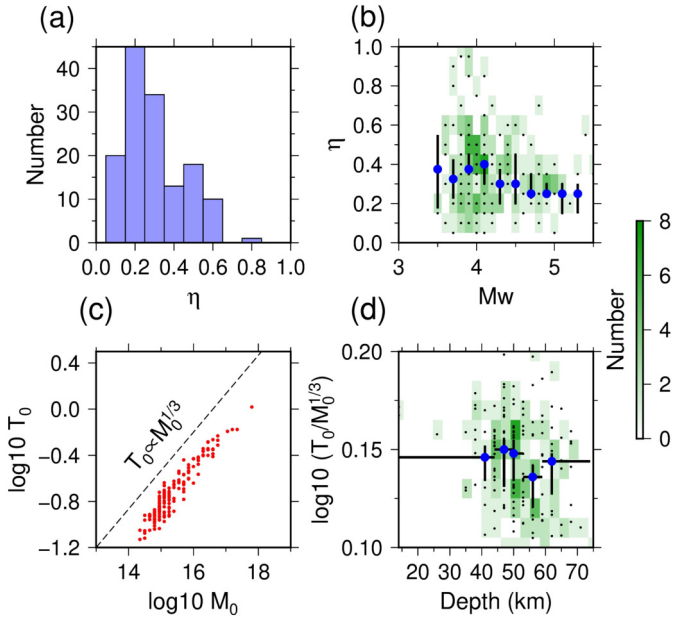

Fig. 5. Derived rupture parameters. Only results with $\Delta AIC > 2$ are shown. (a): Frequency distribution of η. (b): Relationship between η and the moment magnitude. (c): Relationship between seismic moment M_0 and source duration T_0. (d): Relationship between the characteristic source duration $T_0/M_0^{\frac{1}{3}}$ and the centroid depth. Blue circles and vertical lines in (b) and (d) indicate mean values and 90% confidential intervals based on bootstrap re-sampling in each bin with the same number of events. Horizontal lines indicate the depth ranges in the bins. The color scale indicates the number of samples in (b) and (d).

4. Discussion

The results indicate that ruptures of most of the interplate earthquakes primarily propagated in the updip direction. This systematic trend suggests that rupture propagation is not governed by a random process or rupture history but instead is due to permanent structures present in the system. This systematic trend is difficult to explain using small-scale heterogeneities in stress, friction, material properties, and fault geometry. Large-scale properties (much larger than the fault size of an individual earthquake) are required to explain this widespread trend.

A bimaterial fault interface affects the earthquake rupture directions, where two blocks with different elastic properties are located across a fault (Weertman, 1980; Shi and Ben-Zion, 2006). This model predicts that Mode II subshear rupture tends to propagate faster in the direction of motion of the compliant side of the

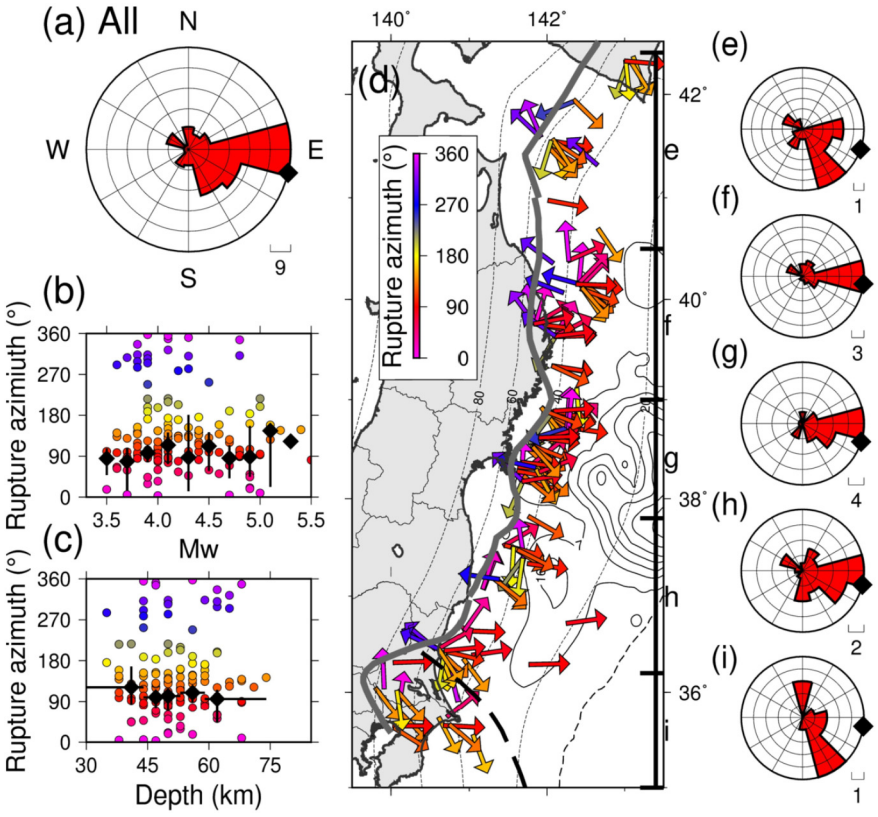

Fig. 6. Estimated rupture propagation directions. Results are indicated for events with a 95% confidence interval of less than 45° and $\Delta AIC > 2$. (a): Frequency distribution of the rupture direction azimuth shown in the form of a rose diagram. The black diamond indicates the updip direction obtained from the mean values of the focal mechanisms. (b) and (c): Relationships between the rupture direction azimuths and moment magnitude and centroid depth, respectively, colored according to the rupture azimuth scale in (d). Diamonds and vertical lines indicate the mean values and the 90% confidential intervals based on bootstrap re-sampling in each bin with the same number of events. (d): Map view showing the rupture direction azimuths. The dashed curve indicates the northeastern limit of the Philippine Sea Plate (Uchida et al., 2009). The gray curve denotes the depth limit of interplate earthquakes on the Pacific plate (Igarashi et al., 2001; Uchida et al., 2009; Kita et al., 2010). Black contours show the coseismic slip distribution of the Tohoku-Oki earthquake (Iinuma et al., 2012). (e)-(i): Frequency distributions of the rupture direction azimuths in the five latitude ranges as shown in (d).

fault, which is supported by observations on the San Andreas Fault (Lengliné and Got, 2011) and laboratory experiments (Anooshehpoor and Brune, 1999). This study used interplate earthquakes that were mostly deeper than 30 km. In this depth range, the footwall material (oceanic crust) is more compliant than the hanging wall material because the hanging wall is the mantle in this depth range (Ito et al., 2004). Therefore, the bimaterial effect predicts that earthquake ruptures will tend to propagate westward (downward), which is the opposite of what we observed. That is, the bimaterial effect alone cannot explain the results of this study.

Determining the cause of the rupture direction is difficult, but the depth dependencies of stress, friction, and pore pressure play essential roles in rupture dynamics in subduction zone. A similar prevalence for updip rupture propagation has been reported for large interplate earthquakes in subduction zones (Kato and Seno, 2003; Chounet et al., 2018) and intraplate earthquakes near the base of the seismogenic zone (Sibson, 1983). One possible cause for the prevalence of updip rupture is a steady creep that occurs along the deeper portion of the plate boundary. The earthquakes analyzed in this study were primarily located near the lower limit of the seismogenic zone (gray curve in Fig. 6), beneath which the plate boundary dislocates aseismically. The contrast in slip velocity between the creeping region and the locked seismogenic patches increases the shear stress along the deeper edge of the locked patches. This facilitates rupture initiation near the deeper edge and propagation in the updip direction, given that the nucleation size is sufficiently smaller than the final rupture area (Kato and Seno, 2003). Numerical modeling of earthquake cycles has shown that some small earthquakes can nucleate near the rheological transition boundary and propagate in a non-preferred direction predicted by the bimaterial effect (Erickson and Day, 2016). The deep aseismic slip and its temporal change that modulate seismicity in the updip seismogenic zone have been observed in the Japan subduction zone from geodetic and repeating earthquake data (Khoshmanesh et al., 2020). Such interaction may be evidence of seismic rupture driven by deeper aseismic slips in the subduction zone.

Upward fluid flow along the plate boundary may play a similar role (Yoshida et al., 2021). Fluids dehydrated from the subducting slab are suggested to migrate upward along the plate boundary because of the permeability anisotropy (Sano et al., 2014). Higher pore pressures result in a higher reduction of fault strength along the deeper portion of the plate boundary. This may contribute to rupture initiation near the deeper edge of the locked patch and propagation in the updip direction. The updip ruptures may open paths for fluids to migrate further upward along the plate interface.

The seismic patches of large earthquakes ($M > 7$) are located in the updip region of the small earthquakes analyzed in this study (Fig. 7). The updip ruptures of small earthquakes may redistribute the shear stress accumulated near the base of the seismogenic zone to the shallow seismic patches of large interplate earthquakes, thereby facilitating the occurrence of large earthquakes. A number of these small earthquakes may represent partial ruptures of the seismic patches of large earthquakes.

The dominant rupture direction has a significant fault-strike component in the northernmost (Fig. 6e) and southernmost (Fig. 6i) regions. Since the trench axis bends near the northernmost region, the bending-related stress and structure may affect the rupture directions of earthquakes in this region. In the southernmost region,

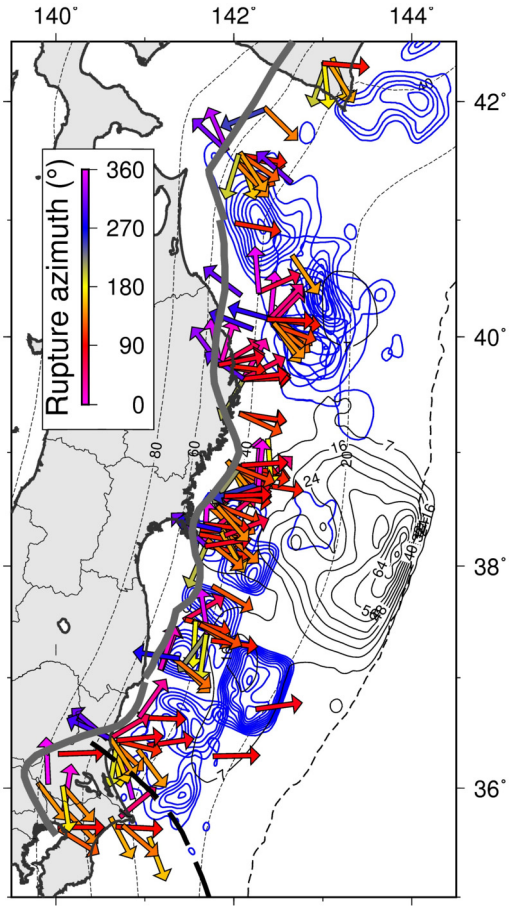

Fig. 7. Seismic patches of large earthquakes ($M > 7$) and rupture propagation directions of small earthquakes (*Mw* 3.5–5). The rupture direction azimuths obtained in this study are shown by arrows and the color scale. Blue contours show slip areas of large earthquakes from Nagai et al. (2001), Yamanaka and Kikuchi (2004), and Kubo and Nishikawa (2020). Black contours show the coseismic slip distribution of the Tohoku-Oki earthquake (Iinuma et al., 2012). Other details are the same as in Fig. 6(d).

the Philippine Sea Plate is subducting from the south, creating a scenario that differs from the other areas. The seismic coupling substantially changes across the northern limit of the Philippines Sea plate (Uchida et al., 2009). The difference in material properties and the state of plate coupling may affect the rupture directivity in this region.

The predominance of updip rupture obtained in this study appears to be the opposite of the downdip ruptures reported for some large earthquakes ($M > 7$) that occurred near the earthquakes analyzed in this study. Fig. 1(b) shows the hypocenters of the $M \sim 7$ interplate earthquakes near the earthquakes analyzed in this study. In the 2011 (M 7.4) Iwate-Oki and (M 7.6) Ibaraki-Oki earthquakes, the ruptures propagated in the updip direction (Kubo et al., 2013; Kubo and Nishikawa, 2020) and were similar to the results presented herein. However, in the 1978 (M 7.4) and 2005 (M 7.2) Miyagi-Oki, and the 2008 (M 7.0) Ibaraki-Oki earthquakes, the ruptures were estimated to have propagated in the downdip direction (Wu et al., 2008; Takiguchi et al., 2011). The bimaterial effect, which facilitates downdip rupture along the deeper portion of the seismogenic zone, may be more dominant for larger earthquakes because the dynamic changes in normal stress increase with propagation distance (Shi and Ben-Zion, 2006). The competition between the bimaterial effect and other effects may cause a diversity in the rupture directions of large earthquakes. The values of η estimated in this study ranged from 0.1 to 0.6, which are significantly smaller than the typical range of V_r/V_s (0.6–0.9) (Geller, 1976). η corresponds to the actual value of V_r/V_s only when the rupture is completely unilateral; otherwise, η should be smaller than the actual V_r/V_s because the fit of the simple unilateral model cannot distinguish between slow and bilateral ruptures. The low values of η obtained in this study suggest that the earthquake ruptures along the Japan trench were directional, but not completely unilateral. η was variable, but appeared to decrease slightly with earthquake size from M_w 3.5 to 5 (Fig. 5b), which may reflect an enhanced bimaterial effect with magnitude that acts against the effect of deeper creep.

Alternatively, the apparent partial discrepancy in some large earthquake rupture directions may be due to temporal changes in the preferable rupture direction. A similar temporal change was reported after the 2004 Parkfield earthquake (Kane et al., 2013). Along the Tohoku-Oki plate boundary, the stress and frictional state were significantly perturbed by the 2011 M 9 Tohoku-Oki earthquake. The results obtained in this study are for the period after the 2011 M 9 Tohoku-Oki earthquake, while the three earthquakes with downdip ruptures (1978 and 2005 Miyagi-Oki and 2008 Ibaraki-Oki earthquakes) occurred before the 2011 Tohoku-Oki earthquake.

There is a possibility that stable creep intruded into the rupture zone of the Tohoku-Oki earthquake during the preparatory process (e.g., Ohtani et al., 2014). In the Miyagi-Oki region, interplate earthquakes occurred in many offshore areas before the Tohoku-Oki earthquake, after which the offshore area was quiet and interplate earthquakes only occurred near the downdip limit of interplate earthquakes. This was probably due to the stress release and locking in the offshore region (e.g., Asano et al., 2011; Uchida and Matsuzawa, 2013). Large-scale postseismic slip followed the Tohoku-Oki earthquake in the down-dip segment (e.g., Tomita et al., 2020) instead of the offshore fault creep before the earthquake. Thus, the occurrence of the 2011 Tohoku-Oki earthquake may have affected the preferential rupture direction of subsequent earthquakes, although it is not clear whether the effect of the Tohoku-Oki earthquake can explain the prevalence of updip rupture throughout the region.

Unfortunately, the temporal changes in rupture directivity cannot be examined before and after the 2011 Tohoku-Oki earthquake using S-net data, as S-net was installed after the 2011 Tohoku-Oki earthquake. Fig. 4(c) shows the difficulty of estimating the rupture propagation direction using stations on land only. However, the earthquake rupture directivities may be constrained solely by stations on land for a few ideal cases (Figs. 2 and 3). To some extent, it may be possible to constrain the rupture directivities of small earthquakes along the Japan trench using stations on land exclusively and assess the above hypothesis for future research.

The results presented herein indicate that the ruptures of most deep interplate earthquakes along the Japan trench had significant directivities. The prevalence of asymmetrical rupture has also been obtained for inland intraplate earthquakes in Japan (Yoshida, 2019). McGuire et al. (2002) conducted global surveys of large earthquakes and concluded that unilateral rupture was predominant. Most studies of small to moderate-sized earthquakes have been conducted primarily by assuming a non-directional model, including estimates of the earthquake stress drop. However, the results of this study suggest that this assumption may be inappropriate for many interplate earthquakes. This issue may be reduced by incorporating the earthquake rupture directivity in the estimation method (Yoshida, 2019; Yoshida et al., 2019). The prevalence of asymmetrical rupture also suggests that acquiring detailed earthquake information (e.g., fault orientation, useful for distinguishing if the earthquake occurred at a plate boundary) is possible for many earthquakes by using directivity.

5. Conclusions

Prevalence of updip ruptures in small earthquakes was observed near the base of the seismogenic zone along the Japan trench after the 2011 *M*9 Tohoku-Oki earthquake. This updip rupture propagation tendency cannot be explained by the effect of a bimaterial interface; instead, the results suggest that deep, steady creep largely affects earthquake ruptures in subduction zones, although upward fluid flow along the plate boundary may also contribute to the ruptures. The updip ruptures redistribute the shear stress accumulated near the base of the seismogenic zone to shallow large seismic patches. In addition, the updip ruptures may open paths for fluids to migrate further upward along the plate interface. They may facilitate the occurrence of shallow megathrust earthquakes. A similar updip rupture propagation tendency was reported for large intraplate earthquakes near the base of the seismogenic zone. However, this study unambiguously demonstrates a similar trend in many small to moderate-sized interplate earthquakes obtained from both land-based and offshore seismic networks.

The present study could scarcely examine shallow interplate earthquakes ($z < 30$ km) that occurred far from the land due to the difficulty in finding appropriate EGF events for the earthquakes. The stress release by the Tohoku-Oki earthquake reduces seismicity in the region. Studies in the future may be able to examine the rupture characteristics of shallow interplate earthquakes by detecting more offshore earthquakes and improving the location accuracy based on the seafloor observation data.

CRediT authorship contribution statement

KY: Conceptualization, Investigation, Writing-Original draft preparation, Writing - Review & Editing
UN: Writing - Review & Editing
HK: Writing - Review & Editing
RT: Data Curation, Writing - Review & Editing
SX: Conceptualization, Writing - Review & Editing

Declaration of competing interest

The authors declare that they have no known competing financial interests or personal relationships that could have appeared to influence the work reported in this paper.

Acknowledgements

We thank the editor (Rebecca Bendick), Manoochehr Shirzaei, and an anonymous reviewer for their constructive comments, which improved the manuscript. This study used hypocenters and S-wave arrival time data reported in the JMA unified catalog. The seismograms were collected and stored by JMA, national universities, and NIED (http://www.hinet.bosai.go.jp/?LANG=en). The figures were created using GMT (Wessel and Smith, 1998). We thank Toru Matsuzawa and Kazuya Tateiwa for discussions about the velocity contrast across the Tohoku-Oki plate boundary. This research was supported by JSPS KAKENHI (Grant Numbers JP 17KK0081 and 20K14569).

Appendix A. Supplementary material

Supplementary material related to this article can be found online at https://doi.org/10.1016/j.epsl.2021.117306.

References

Abercrombie, R.E., 2015. Investigating uncertainties in empirical Green's function analysis of earthquake source parameters. J. Geophys. Res., Solid Earth 120, 1–15. https://doi.org/10.1002/2015JB011984.Received.

Akaike, H., 1974. A new look at the statistical model identification. IEEE Trans. Autom. Control 19, 716–723. https://doi.org/10.1109/TAC.1974.1100705.

Andrews, D.J., 1976. Rupture velocity of plane strain shear cracks. J. Geophys. Res. 81, 5679–5687. https://doi.org/10.1029/JB081i032p05679.

Andrews, D.J., 2013. Objective determination of source parameters and similarity of earthquakes of different size, pp. 259–267.

Anooshehpoor, A., Brune, J.N., 1999. Wrinkle-like Weertman pulse at the interface between two blocks of foam rubber with different velocities. Geophys. Res. Lett. 26, 2025–2028. https://doi.org/10.1029/1999GL900397.

Aoi, S., Asano, Y., Kunugi, T., Kimura, T., Uehira, K., Takahashi, N., Ueda, H., Shiomi, K., Matsumoto, T., Fujiwara, H., 2020. MOWLAS: NIED observation network for earthquake, tsunami and volcano. Earth Planets Space 72. https://doi.org/10.1186/s40623-020-01250-x.

Asano, Y., Saito, T., Ito, Y., Shiomi, K., Hirose, H., 2011. Spatial distribution and focal mechanisms of aftershocks of the 2011 off the Pacific coast of Tohoku earthquake. Earth Planets Space 63, 669–673. https://doi.org/10.5047/eps.2011.06.016.

Chounet, A., Vallée, M., Causse, M., Courboulex, F., 2018. Global catalog of earthquake rupture velocities shows anticorrelation between stress drop and rupture velocity. Tectonophysics 733, 148–158. https://doi.org/10.1016/j.tecto.2017.11.005.

Erickson, B.A., Day, S.M., 2016. Bimaterial effects in an earthquake cycle model using rate-and-state friction. J. Geophys. Res., Solid Earth 121, 2480–2506. https://doi.org/10.1002/2015JB012470.

Geller, R.J., 1976. Scaling relations for earthquake source parameters and magnitudes. Bull. Seismol. Soc. Am. 66, 1501–1523.

Harris, R.A., Day, S.M., 2005. Material contrast does not predict earthquake rupture propagation direction. Geophys. Res. Lett. 32, 1–4. https://doi.org/10.1029/2005GL023941.

Hasegawa, A., Yoshida, K., Asano, Y., Okada, T., Iinuma, T., Ito, Y., 2012. Change in stress field after the 2011 great Tohoku-Oki earthquake. Earth Planet. Sci. Lett. 355–356, 231–243. https://doi.org/10.1016/j.epsl.2012.08.042.

Haskell, N.A., 1964. Total energy and energy spectral density of elastic wave radiation from propagating faults. Bull. Seismol. Soc. Am. 54, 1811–1841.

Igarashi, T., Matsuzawa, T., Umino, N., Hasegawa, A., 2001. Spatial distribution of focal mechanisms for interplate and intraplate earthquakes associated with the subducting Pacific plate beneath the northeastern Japan arc: a triple-planed deep seismic zone. J. Geophys. Res., Solid Earth 106, 2177–2191. https://doi.org/10.1029/2000jb900386.

Iinuma, T., Hino, R., Kido, M., Inazu, D., Osada, Y., Ito, Y., Ohzono, M., Tsushima, H., Suzuki, S., Fujimoto, H., Miura, S., 2012. Coseismic slip distribution of the 2011 off the Pacific coast of Tohoku earthquake (M 9.0) refined by means of seafloor geodetic data. J. Geophys. Res., Solid Earth 117. https://doi.org/10.1029/2012JB009186.

Ito, A., Fujie, G., Tsuru, T., Kodaira, S., Nakanishi, A., Kaneda, Y., 2004. Fault plane geometry in the source region of the 1994 Sanriku-oki earthquake. Earth Planet. Sci. Lett. 223, 163–175. https://doi.org/10.1016/j.epsl.2004.04.007.

Kanamori, H., Anderson, D., 1975. Theoretical basis of some empirical relations in seismology. Bull. Seismol. Soc. Am. 65, 1073–1095.

Kane, D.L., Shearer, P.M., Goertz-Allmann, B.P., Vernon, F.L., 2013. Rupture directivity of small earthquakes at parkfield. J. Geophys. Res., Solid Earth 118, 212–221. https://doi.org/10.1029/2012JB009675.

Kato, N., Seno, T., 2003. Hypocenter depths of large interplate earthquakes and their relation to seismic coupling. Earth Planet. Sci. Lett. 210, 53–63. https://doi.org/10.1016/S0012-821X(03)00141-9.

Khoshmanesh, M., Shirzaei, M., Uchida, N., 2020. Deep slow-slip events promote seismicity in northeastern Japan megathrust. Earth Planet. Sci. Lett. 540, 116261. https://doi.org/10.1016/j.epsl.2020.116261.

Kita, S., Okada, T., Hasegawa, A., Nakajima, J., Matsuzawa, T., 2010. Anomalous deepening of a seismic belt in the upper-plane of the double seismic zone in the Pacific slab beneath the Hokkaido corner: possible evidence for thermal shielding caused by subducted forearc crust materials. Earth Planet. Sci. Lett. 290, 415–426. https://doi.org/10.1016/j.epsl.2009.12.038.

Kubo, H., Asano, K., Iwata, T., 2013. Source-rupture process of the 2011 Ibaraki-oki, Japan, earthquake (Mw 7.9) estimated from the joint inversion of strong-motion and GPS data: relationship with seamount and Philippine Sea plate. Geophys. Res. Lett. 40, 3003–3007. https://doi.org/10.1002/grl.50558.

Kubo, H., Nishikawa, T., 2020. Relationship of preseismic, coseismic, and postseismic fault ruptures of two large interplate aftershocks of the 2011 Tohoku earthquake with slow-earthquake activity. Sci. Rep. 10. https://doi.org/10.1038/s41598-020-68692-x.

Lengliné, O., Got, J.L., 2011. Rupture directivity of microearthquake sequences near parkfield, California. Geophys. Res. Lett. 38. https://doi.org/10.1029/2011GL047303.

Ligorría, J.P., Ammon, C.J., 1999. Iterative deconvolution and receiver-function estimation. Bull. Seismol. Soc. Am. 89, 1395–1400.

McGuire, J.J., Zhao, L., Jordan, T.H., 2002. Predominance of unilateral rupture for a global catalog of large earthquake. Bull. Seismol. Soc. Am. 92, 3309–3317. https://doi.org/10.1785/0120010293.

Nagai, R., Kikuchi, M., Yamanaka, Y., 2001. Comparative study on the source processes of recurrent large earthquakes in Sanriku-oki region: the 1968 Tokachi-oki earthquake and the 1994 Sanriku-oki earthquake. Zisin 54, 267–280. https://doi.org/10.4294/zisin1948.54.2_267.

Nakajima, J., Hirose, F., Hasegawa, A., 2009. Seismotectonics beneath the Tokyo metropolitan area, Japan: effect of slab-slab contact and overlap on seismicity. J. Geophys. Res., Solid Earth 114, B08309. https://doi.org/10.1029/2008JB006101.

National Research Institute for Earth Science and Disaster Resilience, 2019a. NIED Hi-net. Natl. Res. Inst. Earth Sci. Disaster Resil. https://doi.org/10.17598/NIED.0003.

National Research Institute for Earth Science and Disaster Resilience, 2019b. NIED F-net. Natl. Res. Inst. Earth Sci. Disaster Resil. https://doi.org/10.17598/NIED.0005.

National Research Institute for Earth Science and Disaster Resilience, 2019c. NIED V-net. Natl. Res. Inst. Earth Sci. Disaster Resil. https://doi.org/10.17598/NIED.0006.

National Research Institute for Earth Science and Disaster Resilience, 2019d. NIED S-net. Natl. Res. Inst. Earth Sci. Disaster Resil. https://doi.org/10.17598/NIED.0007.

Ohtani, M., Hirahara, K., Hori, T., Hyodo, M., 2014. Observed change in plate coupling close to the rupture initiation area before the occurrence of the 2011 Tohoku earthquake: implications from an earthquake cycle model. Geophys. Res. Lett. 41, 1899–1906. https://doi.org/10.1002/2013GL058751.

Sano, Y., Hara, T., Takahata, N., Kawagucci, S., Honda, M., Nishio, Y., Tanikawa, W., Hasegawa, A., Hattori, K., 2014. Helium anomalies suggest a fluid pathway from mantle to trench during the 2011 Tohoku-Oki earthquake. Nat. Commun. 5. https://doi.org/10.1038/ncomms4084.

Sato, T., Hirasawa, T., 1973. Body wave spectra from propagating shear cracks. J. Phys. Earth. https://doi.org/10.4294/jpe1952.21.415.

Shi, Z., Ben-Zion, Y., 2006. Dynamic rupture on a bimaterial interface governed by slip-weakening friction. Geophys. J. Int. 165, 469–484. https://doi.org/10.1111/j.1365-246X.2006.02853.x.

Sibson, R.H., 1983. Continental fault structure and the shallow earthquake source. J. Geol. Soc. London. 140, 741–767. https://doi.org/10.1144/gsjgs.140.5.0741.

Takagi, R., Uchida, N., Nakayama, T., Azuma, R., Ishigami, A., Okada, T., Nakamura, T., Shiomi, K., 2019. Estimation of the orientations of the S-net cabled ocean-bottom sensors. Seismol. Res. Lett. 90, 2175–2187. https://doi.org/10.1785/0220190093.

Takiguchi, M., Asano, K., Iwata, T., 2011. The comparison of source models of repeating subduction-zone earthquakes estimated using broadband strong motion records-1982 and 2008 Ibaraki-ken-oki M7 earthquakes. Zisin. https://doi.org/10.4294/zisin.63.223.

Tomita, F., Iinuma, T., Ohta, Y., Hino, R., Kido, M., Uchida, N., 2020. Improvement on spatial resolution of a coseismic slip distribution using postseismic geodetic data through a viscoelastic inversion. Earth Planets Space 72, 84. https://doi.org/10.1186/s40623-020-01207-0.

Uchida, N., Nakajima, J., Hasegawa, A., Matsuzawa, T., 2009. What controls interplate coupling?: Evidence for abrupt change in coupling across a border between two overlying plates in the NE Japan subduction zone. Earth Planet. Sci. Lett. 283, 111–121. https://doi.org/10.1016/j.epsl.2009.04.003.

Uchida, N., Matsuzawa, T., 2013. Pre- and postseismic slow slip surrounding the 2011 Tohoku-oki earthquake rupture. Earth Planet. Sci. Lett. 374, 81–91. https://doi.org/10.1016/j.epsl.2013.05.021.

Ueno, H., Hatakeyama, S., Aketagawa, T., Funasaki, J., Hamada, N., 2002. Improvement of hypocenter determination procedures in the Japan meteorological agency. Q. J. Seismol. 65, 123–134 (in Japanese).

Weertman, J., 1980. Unstable slippage across a fault that separates elastic media of different elastic constants. J. Geophys. Res. 85, 1455. https://doi.org/10.1029/JB085iB03p01455.

Wu, C., Koketsu, K., Miyake, H., 2008. Source processes of the 1978 and 2005 Miyagi-oki, Japan earthquakes: repeated rupture of asperities over successive large earthquakes. J. Geophys. Res., Solid Earth 113. https://doi.org/10.1029/2007JB005189.

Yamanaka, Y., Kikuchi, M., 2004. Asperity map along the subduction zone in northeastern Japan inferred from regional seismic data. J. Geophys. Res., Solid Earth 109. https://doi.org/10.1029/2003JB002683.

Ye, L., Lay, T., Kanamori, H., Rivera, L., 2016. Rupture characteristics of major and great (Mw $\geq$ 7.0) megathrust earthquakes from 1990 to 2015: 1. Source parameter scaling relationships. J. Geophys. Res., Solid Earth 121, 826–844. https://doi.org/10.1002/2015JB012426.

Yoshida, K., 2019. Prevalence of asymmetrical rupture in small earthquakes and its effect on the estimation of stress drop: a systematic investigation in inland Japan. Geosci. Lett. 6. https://doi.org/10.1186/s40562-019-0145-z.

Yoshida, K., Saito, T., Emoto, K., Urata, Y., Sato, D., 2019. Rupture directivity, stress drop, and hypocenter migration of small earthquakes in the Yamagata-Fukushima border swarm triggered by upward pore-pressure migration after the 2011 Tohoku-Oki earthquake. Tectonophysics 769. https://doi.org/10.1016/j.tecto.2019.228184.

Yoshida, K., Noda, H., Nakatani, M., Shibazaki, B., 2021. Backward earthquake ruptures far ahead of fluid invasion: insights from dynamic earthquake-sequence simulations. Tectonophysics 816, 229038. https://doi.org/10.1016/j.tecto.2021.229038.